# Landscape response to tectonic forcing: Digital elevation model analysis of stream profiles in the Mendocino triple junction region, northern California

**Noah P. Snyder*** **Kelin X. Whipple** } *Department of Earth, Atmospheric, and Planetary Sciences, Massachusetts Institute of Technology, Cambridge, Massachusetts 02139-4307, USA*

**Gregory E. Tucker** *Department of Civil and Environmental Engineering, Massachusetts Institute of Technology, Cambridge, Massachusetts 02139-4307, USA*

**Dorothy J. Merritts** *Department of Geosciences, Franklin and Marshall College, Lancaster, Pennsylvania 17604-3003, USA*

## ABSTRACT

**The topographic evolution of orogens is fundamentally dictated by rates and patterns of bedrock-channel incision. Quantitative field assessments of process-based laws are needed to accurately describe landscape uplift and denudation in response to tectonics and climate. We evaluate and calibrate the shear stress (or similar unit stream-power) bedrock-incision model by studying stream profiles in a tectonically active mountain range. Previous work on emergent marine terraces in the Mendocino triple junction region of northern California provides spatial and temporal control on rock-uplift rates. Digital elevation models and field data are used to quantify differences in landscape morphology associated with along-strike northwest to southeast changes in tectonic and climatic conditions. Analysis of longitudinal profiles supports the hypothesis that the study-area channels are in equilibrium with current uplift and climatic conditions, consistent with theoretical calculations of system response time based on the shear-stress model. Within uncertainty, the profile concavity ($\theta$) of the trunk streams is constant throughout the study area ($\theta \approx 0.43$), as predicted by the model. Channel steepness correlates with uplift rate. These data help constrain the two key unknown model parameters, the coefficient of erosion ($K$) and the exponent associated with channel gradient ($n$). This analysis shows that $K$ cannot be treated as a constant throughout the study area, despite generally homogeneous substrate properties. For a reasonable range of slope-exponent values ($n$), best-fit values of $K$ are positively correlated with uplift rate. This correlation has important implications for landscape-evolution models and likely reflects dynamic adjustment of $K$ to tectonic changes, due to variations in orographic precipitation, and perhaps channel width, sediment load, and frequency of debris flows. The apparent variation in $K$ makes a unique value of $n$ impossible to constrain with present data.**

**Keywords: channel geometry, digital elevation models, erosion rates, fluvial erosion, geomorphology, landscape evolution.**

## INTRODUCTION

The potential for dynamic interactions among surficial processes, crustal processes, and climate has received broad interdisciplinary attention in recent years (e.g., Molnar and England, 1990; Beaumont et al., 1992; Raymo and Ruddiman, 1992; Hoffman and Grotzinger, 1993; Koons, 1995). This interest has helped spur numerical modeling attempts to analyze the interplay of these large-scale processes on topographic evolution of mountain ranges (e.g., Anderson, 1994; Tucker and Slingerland, 1994; Kooi and Beaumont, 1996). While considerable progress has been made, these modeling efforts have been hampered by the lack of data on fluvial bedrock-erosion rates and processes, as noted by Merritts and Ellis (1994). In particular, many aspects of the dynamic response of bedrock channels to tectonic forcing are not known quantitatively (Whipple and Tucker, 1999).

Bedrock channels play a key role in landscape evolution. The ability of streams to incise through bedrock ultimately sets the rate of lowering of a landscape, and therefore mass removal, in actively rising mountainous regions. Several recent studies of bedrock channels have focused on erosion processes and morphology (e.g., Foley, 1980; Howard and Kerby, 1983; Hancock et al., 1998; Pazzaglia et al., 1998; Sklar and Dietrich, 1998; Wohl, 1998; Whipple et al., 2000). We build on this research in an area of known, spatially variable tectonic rock-uplift rates, where dynamic stream response can be quantified (Merritts and Vincent, 1989). The nature and timing of channel response are crucial unknowns in our ability to describe quantitatively many aspects of landscape evolution and the geologic record, including hillslope response, sediment flux, and transmission of base-level signals through a watershed. In this paper we evaluate and calibrate a model for channel longitudinal-profile evolution in a tectonically active mountain range. The effort combines testing of certain model predictions with field constraints on key model parameters.

Various models based on the postulate that bedrock-channel incision rate is proportional to shear stress or unit stream power have been proposed (e.g., Howard and Kerby, 1983). Although these models have been applied to field data (Howard and Kerby, 1983; Seidl and Dietrich, 1992; Rosenbloom and Anderson, 1994; Pazzaglia et al., 1998; Sklar and Dietrich, 1998; Talling and Sowter, 1998; Weissel and Seidl, 1998; Stock and Montgomery, 1999), they remain relatively untested and their parameters poorly constrained. More quantitative field tests of these models are required, particularly in active tectonic settings. Even in the simplest form, the dynamics of landscape evolution

*E-mail: noahp@mit.edu.

*GSA Bulletin*; August 2000; v. 112; no. 8; p. 1250–1263; 10 figures; 3 Tables.

driven by the shear-stress model depend on at least two key unknown parameters: the coefficient of erosion and the exponent associated with channel gradient (Whipple and Tucker, 1999). In field areas where substrate properties are invariant, and climate and uplift histories are known, these parameters may be estimated from field and map data.

We study 21 small coastal streams in the Mendocino triple junction region of northern California, where the lithologic, climatic, and tectonic conditions can be constrained both spatially and temporally. Highly fractured mudstone and sandstone underlie the area (McLaughlin et al., 1994); variations in lithologic resistance are only on a local scale. Late Quaternary climate fluctuations were subdued in the maritime region (Johnson, 1977), although the orographic effect of topography causes important, quantifiable precipitation differences. The previous work of Merritts and collaborators on flights of emergent marine terraces in the Mendocino triple junction region shows that along the coast, late Pleistocene and Holocene rock-uplift rates vary over nearly an order of magnitude, from 0.5 mm $yr^{-1}$ to 4 mm $yr^{-1}$ (Merritts and Bull, 1989; Merritts and Vincent, 1989; Merritts, 1996). In addition, high rock-uplift rates only began ca. 100 ka (Merritts and Bull, 1989), affording the opportunity to investigate channel response to a change in tectonic forcing.

We use data from digital elevation models (DEMs), field surveys, and topographic maps. DEMs have been used by numerous workers to analyze fluvial channels (e.g., Tarboton et al., 1991; Dietrich et al., 1993; Montgomery and Foufoula-Georgiou, 1993; Willgoose, 1994; Moglen and Bras, 1995; Tucker, 1996; Sklar and Dietrich, 1998; Weissel and Seidl, 1998). Comparisons among various digital topographic analysis techniques are provided, and these methods are tested using topographic maps and field surveys for a few basins. The goal of this analysis is to critically evaluate the applicability of DEMs to study of bedrock channels in the context of the shear-stress incision model. DEMs are used to quantify channel longitudinal profile form, drainage area, and local slope, focusing on the bedrock-channel dominated part of the system. Field measurements and observations are used to constrain the relationship between bedrock-channel width and drainage area, and to characterize local channel morphology.

This paper is an attempt to evaluate and constrain the shear-stress model, using DEMs and field data, in a field site where the tectonic history is known. Specifically, we present data quantifying: (1) the concavity and steepness of trunk streams in study-area drainages and their dependence on uplift rate; (2) variations in the coefficient of erosion in concert with differences in uplift rate; (3) the degree of nonlinearity in the relation between channel slope and incision rate; and (4) the time scale of channel response to a change in tectonic conditions.

These analyses yield a picture of landscape evolution in a bedrock-channel–dominated, young mountain range. We begin by developing the theoretical basis of the shear-stress model, with reference to the possibilities for constraining model parameters with field and DEM data. Second, the tectonic history, lithology, climate, and channel morphology of the Mendocino triple junction study area are described. Third, the applicability of the theory to the field area is carefully evaluated. Next, the methods and results of the longitudinal-profile analysis are reviewed and presented. Finally, the implications of the results are discussed in terms of channel-response processes and time scale.

## THEORETICAL FRAMEWORK

Many workers have modeled detachment-limited bedrock-channel incision using a form of the shear-stress (or similar unit stream-power) model, in which incision rate is given by a power function of drainage area and channel slope (e.g., Howard and Kerby, 1983; Seidl and Dietrich, 1992; Anderson, 1994; Howard, 1994; Moglen and Bras, 1995; Tucker, 1996; Stock and Montgomery, 1999; Whipple and Tucker, 1999). Here we provide a brief synopsis of the derivation of this law. The shear-stress model is used to describe the evolution of bedrock-channel longitudinal profiles. The objective of this section is to establish how measurements of topography and channel form in real landscapes can be used to constrain model parameters.

### Shear-Stress Incision Model

The shear-stress incision model is predicated on the hypothesis that bedrock-channel-erosion rate ($E$), in volume per unit channel area per time, is a power-law function of basal shear stress ($\tau_b$):

$$E = k_b \tau_b^{\,a}, \tag{1}$$

where $k_b$ is a dimensional coefficient dependent on dominant erosion process, rock resistance, and possibly sediment load, and $a$ is a positive, process-dependent constant. Theoretical predictions for the value of $a$ vary from 1 for a linear-erosion process in easily eroded material (Howard and Kerby, 1983) to ~5/2 for impact abrasion (Foley, 1980; Hancock et al., 1998; Whipple et al., 2000). Combining the assumptions of conservation of mass (water), and steady, uniform flow, the following expression for basal shear stress ($\tau_b$) is obtained:

$$\tau_b = \rho C_f^{1/3} \left[ \frac{gSQ}{W} \right]^{2/3}, \tag{2}$$

where $\rho$ is density of water, $C_f$ is a dimensionless friction factor, $g$ is gravitational acceleration, $S$ is local channel slope ($dz/dx$), $Q$ is a characteristic stream discharge (Wolman and Miller, 1960), and $W$ is a characteristic channel width. Next, a relationship for basin hydrology is assumed:

$$Q = k_q A^c, \tag{3}$$

where $A$ is upstream drainage area, $k_q$ is a dimensional coefficient, and $c$ is a positive constant, the value of which is approximately unity or slightly less (Dunne and Leopold, 1978; Pazzaglia et al., 1998), particularly for small, steep drainages, such as those studied here. Then, a relationship for downstream increase in channel width with discharge is assumed, and combined with equation 3:

$$W = k_w Q^b = k_w k_q^{\,b} A^{bc}, \tag{4}$$

where $k_w$ is a dimensional coefficient and $b$ is a positive constant, empirically observed to be ~0.5 in alluvial rivers (Leopold and Miller, 1956). The products $k_w k_q^{\,b}$ and $bc$ may be found from drainage-area data and field measurements of channel width. Finally, equations 1–4 are combined to obtain the well-known shear-stress incision law,

$$E = KA^m S^n, \tag{5}$$

with the relations

$$K = k_b k_w^{\,-2a/3} k_q^{\,2a(1-b)/3} \rho^a g^{2a/3}; \tag{6}$$

$$m = (2ac/3)(1-b); \tag{7}$$

$$n = 2a/3; \tag{8}$$

and

$$m/n = c(1-b). \tag{9}$$

Equations 5–9 highlight the key unconstrained parameters in the shear-stress model. Equation 9 indicates that the ratio $m/n$ is expected to be constant for a broad set of shear-stress–driven fluvial incision processes (Whipple and Tucker, 1999), an important, testable model prediction. For the typical, empirically determined values of $b$ and $c$ (equations 3 and 4), the value of $m/n$ is ~0.5. However, the exponent $b$ is only known well for alluvial channels, and further means of constraining this ratio by measuring channel width as a function of drainage area (equation 4) are discussed in the following. This relation reduces the modeling problem to two key unknowns: $K$ and $n$. The slope exponent ($n$) depends on the mechanics of erosion processes ($a$), as discussed here. Whipple and Tucker (1999) show that the value of $n$ exerts strong control on equilibrium channel slope, equilibrium topographic relief, transient profile form, and response time scale. We now briefly investigate the factors that control the value of $K$.

### Erosion Coefficient

The erosion coefficient ($K$) is not well calibrated, but one study (Stock and Montgomery, 1999) has presented evidence that $K$ varies over orders of magnitude among different study areas. $K$ is a dimensional coefficient with units of meters$^{1-2m}$ yr$^{-1}$. A wide variety of factors probably influence $K$, including rock strength, channel bed material, channel width, runoff, and debris-flow frequency. Although the frequency of debris flows in a fluvially dominated channel may influence $K$, the shear-stress incision model is likely to be inadequate in debris-flow–dominated channels (Howard, 1998; Stock and Dietrich, 1998). In addition, $K$, or specifically $k_b$ (equation 1), may be a function of sediment load, with large sediment concentrations protecting the bed, as argued by Sklar and Dietrich (1998). We revisit this issue later in this paper. Within an area of relatively uniform lithology, $K$ (or an analogous erodibility parameter) has often been modeled as constant in both space and time (e.g., Seidl and Dietrich, 1992; Anderson, 1994; Kooi and Beaumont, 1996). Holding $K$ constant in a model of landscape response to tectonic forcing includes the implicit assumption that channel gradient is the only variable that is free to adjust to changes in rock-uplift rate. However, many of the factors that control $K$ are likely to adjust during the evolution of a mountain range. For example, higher uplift rates are likely to lead to higher topography, which leads to increased orographic precipitation, presumably increasing $k_q$ and therefore $K$ (equation 6). In addition, channels may narrow in response to an increase in the rate of relative base-level fall (decreasing $k_w$ and increasing $K$), or may become more alluviated in response to changes in sediment flux (perhaps decreasing $k_b$ and $K$; equation 6). We present evidence here that the coefficient of erosion ($K$) may indeed vary in response to tectonic forcing. We also place some preliminary constraints on the relative importance of adjustments in channel width, bed configurations, and orographic precipitation.

### Steady-State Longitudinal Profiles

The shear-stress incision model can be combined with a statement of conservation of mass to analyze the rate of change of river-bed elevation ($dz/dt$), given by a competition between uplift and erosion (e.g., Howard, 1994):

$$dz/dt = U - E = U - KA^mS^n, \quad (10)$$

where $U$ is the rock uplift rate relative to base level. In the case of a steady-state landscape ($dz/dt = 0$), equation 10 can be solved for equilibrium slope ($S_e$):

$$S_e = (U/K)^{1/n}A^{-m/n}, \quad (11)$$

where, for cases of uniform $U$ and $K$, $m/n$ dictates the concavity of the equilibrium profile, and likewise the coefficient $(U/K)^{1/n}$ dictates equilibrium profile steepness. The power-function relation implied by equation 11 has been observed empirically in many different geologic settings, with stream gradient described by

$$S = k_sA^{-\theta}. \quad (12)$$

The exponent, $\theta$ (the concavity index), and coefficient, $k_s$ (the steepness index), can be measured directly by regression of slope and area data. The concavity index ($\theta$) is generally found to be between 0.3 and 0.6 (Hack, 1957; Flint, 1974; Willgoose et al., 1990; Tarboton et al., 1991; Moglen and Bras, 1995; Slingerland et al., 1998), but values to 1.1 have been measured in some channels (Sklar and Dietrich, 1998). The coefficient $k_s$ is similar in principle to the stream-gradient index developed by Hack (1973), but more general. In any analysis of stream longitudinal profiles, the relationships implied by equations 11 and 12:

$$\theta = m/n, \quad (13)$$

and

$$k_s = (U/K)^{1/n}, \quad (14)$$

hold true if and only if (1) the river profile is in steady state with respect to current climatic and uplift conditions; and (2) both uplift rate ($U$) and coefficient of erosion ($K$) are uniform through the channel reach. Where these conditions are met, the parameters $(U/K)^{1/n}$ and $m/n$ can be estimated directly through regressions of channel-gradient and drainage-area data. In such cases, the degree of correlation between channel steepness and rock-uplift rate can be used to place important constraints on shear-stress model parameters. If $K$ is constant throughout the study area, a unique value of $n$ may be determined directly. In addition, the model prediction that the $m/n$ ratio is a constant, largely dictated by the relationship between channel width and drainage area (equation 4), can be tested directly. Whipple and Tucker (1999) derived an expression for channel response time to changes in rock-uplift rate. Predicted response times can be tested where information on the rock-uplift history is available, such as in the Mendocino triple junction region. In the discussion section of this paper, we modify the channel response-time equation give by Whipple and Tucker to account for possible changes in $K$ in concert with increased uplift rate and compare predicted response times to uplift history (Merritts and Bull, 1989).

## FIELD AREA

The King Range is an area of rugged relief at the northern terminus of the San Andreas fault in northern California (Fig. 1). The study area consists of a subparallel series of 21 small coastal drainage basins from Cape Mendocino in the north, through the King Range to Fort Bragg in the south (Fig. 2; Table 1), previously studied by Merritts and Vincent (1989). Late Pleistocene and Holocene rock-uplift rates vary nearly an order of magnitude along this 120 km transect, from ~3 mm yr$^{-1}$ near the Bear River, to 4 mm yr$^{-1}$ in the King Range, to ~0.5 mm yr$^{-1}$ at Fort Bragg (Fig. 3) (McLaughlin et al., 1983; Merritts and Bull, 1989; Merritts, 1996). These uplift rates are obtained from radiocarbon dating of fossil shells sampled either from in-place growth positions on emergent marine platforms or from within intertidal marine sediments overlying marine platforms (Merritts and Bull, 1989; Merritts, 1996). Marine platforms and cover-bed sediments are numerous throughout the study area, forming flights of uplifted late Pleistocene and Holocene marine terraces that are correlated with a eustatic sea-level curve

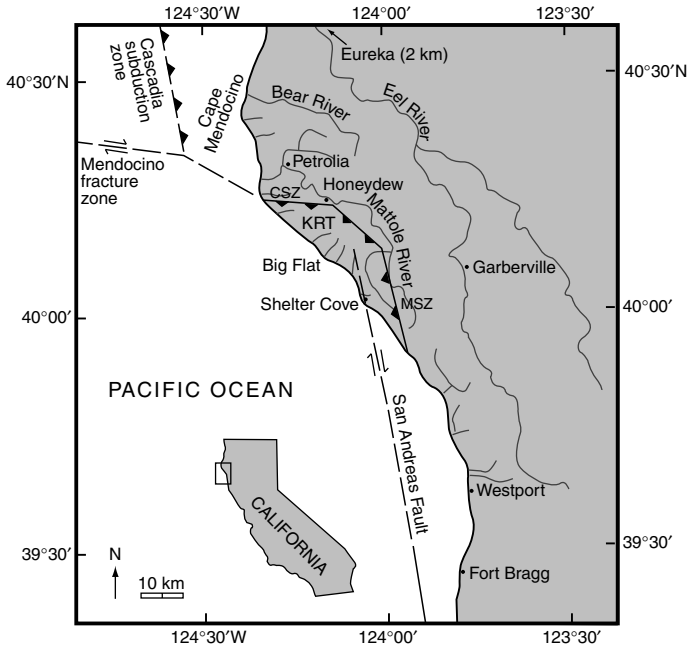


**Figure 1. The Mendocino triple junction region study area, including the King Range terrane (KRT). Eastern and northern boundaries of the terrane are the Mattole and Cooskie shear zones (MSZ and CSZ), respectively (McLaughlin et al., 1994). Modified from Merritts and Vincent (1989), Merritts (1996), and Prentice et al. (1999).**

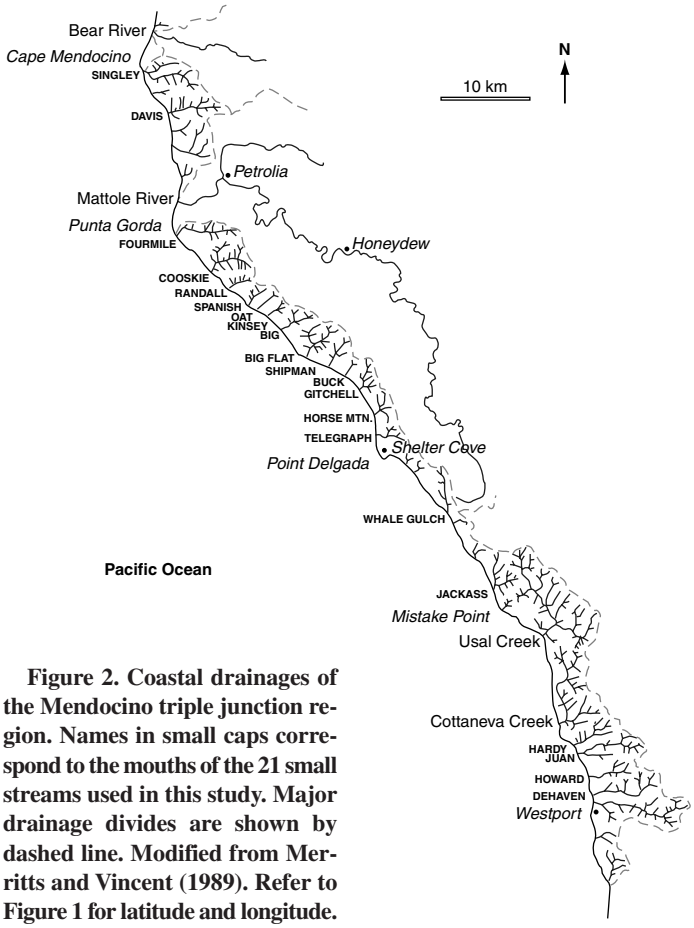


**Figure 2. Coastal drainages of the Mendocino triple junction region. Names in small caps correspond to the mouths of the 21 small streams used in this study. Major drainage divides are shown by dashed line. Modified from Merritts and Vincent (1989). Refer to Figure 1 for latitude and longitude.**

in order to extend the uplift-rate record back to 330 ka, beyond the range of radiocarbon dating (Merritts and Bull, 1989). The terraces do not show any signs of significant coast-perpendicular tilting, indicating that the uplift rates are approximately uniform within each study-area basin. Much of our analysis hinges upon these uplift-rate data, which are an important potential source of uncertainty (Merritts and Bull, 1989; Merritts, 1996). The extremely high uplift rate of the King Range terrane, between the Cooskie and Mattole shear zones, is related to plate boundary interactions around the northward-propagating Mendocino triple junction (McLaughlin et al., 1994; Merritts, 1996; Prentice et al., 1999).

The uplift-rate data and local structural geology provide a rough means of dividing the study area into four distinct zones, from north to south, the northern transition zone (Singley Creek to Cooskie Creek), the King Range high-uplift zone (Randall Creek to Gitchell Creek), the intermediate-uplift zone (Horse Mountain Creek to Whale Gulch), and the low-uplift zone (Jackass Creek to Dehaven Creek; Fig. 3). The northern and high-uplift zones underwent an acceleration in uplift rates after 96 ka from low-uplift-zone conditions (<1 mm $yr^{-1}$) to 3–4 mm $yr^{-1}$ (Merritts and Bull, 1989). Uplift rates in the southern part of the study area have been constant for at least the past 330 k.y. (Merritts and Bull, 1989). The transition in tectonic setting from low- to high-uplift rates provides the opportunity to isolate the effects of this change by comparison of topographic data between two otherwise generally similar regions.

Bedrock lithology in the study area consists of Tertiary and Cretaceous marine sandstones and mudstones of the Franciscan assemblage (Beutner et al., 1980; McLaughlin et al., 1994). In general, the rocks are jointed on the submeter scale and easily eroded, although local variations in resistance provide some areas of small-scale lithologic control on channel characteristics. In addition, the large shear zones that surround the King Range terrane produce differences in the level of deformation and jointing of the rocks (Figs. 1 and 3; Beutner et al., 1980; McLaughlin et al., 1994). Although heterogeneous at the small scale, the rocks of the study area show no clear large-scale variations in lithologic resistance between catchments (S. Ellen, unpublished data; Merritts and Vincent, 1989) although this possibility cannot entirely be ruled out.

The 21 study-area drainage basins are variable-bed-gradient bedrock streams (morphologic terminology of Wohl, 1998). The basins range from 3.1 to 20.8 $km^2$ in area. The streams are steep and narrow. Generally, the local stream-bed morphology varies from cobble to sand plane bed near the mouths of the larger drainages to a locally variable mix of step-pool, boulder-cascade, bedrock, and colluvial conditions in the higher parts of the basins (classification scheme of Montgomery and Buffington, 1997). Strath and fill terraces are common in many of the drainages.

In the higher, steeper channel reaches (bed slope > 1°–2°) away from channel mouths, the bed composition of the streams is a mix of exposed bedrock and scattered alluvial and colluvial deposits (Fig. 4A). In heavily jointed areas, plucking along joint planes appears to be the dominant erosion process, evidenced by numerous unweathered and only slightly abraded exposed joint surfaces. Streambed exposures of massive bedrock (joint spacing > 0.3 m) generally are polished, and probably sculpted by bedload abrasion (Fig. 4B). Discontinuous coarse-grained alluvial deposits are common throughout the basins. Occasional debris-flow deposits are found locally, particularly higher in the basins. Debris flows probably contribute to channel incision, but the significance of this contribution is unknown at present. Landslide deposits are common at sites of recent mass-wasting activity on steep side slopes throughout the study drainages. These colluvial deposits appear to be reworked rapidly and retransported by flu-

TABLE 1. TOPOGRAPHIC DATA FOR THE 21 STUDY-AREA CHANNELS

| No. | Basin name | Distance* (km) | Uplift rate, $U$ (m yr$^{-1}$) | Drainage area $A$ (km$^2$) | Basin length $L$ (m) | Critical distance† $x_c$ (m) | ± 2σ§ | $k_s$, for θ = 0.43§ | $K$, for $n$ = 1 (m$^{0.14}$ yr$^{-1}$)§ |
|---|---|---|---|---|---|---|---|---|---|
| 1 | Singley | 6.2 | 0.003 | 20.8 | 8939 | 367 | 0.37 ± 0.14 | 60 | $5.0 \times 10^{-5}$ |
| 2 | Davis | 12.0 | 0.003 | 17.7 | 8851 | 544 | 0.29 ± 0.16 | 64 | $4.7 \times 10^{-5}$ |
| 3 | Fourmile | 24.7 | 0.0035 | 13.5 | 9568 | 440 | 0.58 ± 0.11 | 56 | $6.3 \times 10^{-5}$ |
| 4 | Cooskie | 30.6 | 0.0035 | 18.1 | 7398 | 342 | 0.43 ± 0.12 | 48 | $7.3 \times 10^{-5}$ |
| 5 | Randall | 33.5 | 0.004 | 4.8 | 3743 | 350 | 0.45 ± 0.11 | 74 | $5.4 \times 10^{-5}$ |
| 6 | Spanish | 36.3 | 0.004 | 4.8 | 4304 | 472 | 0.44 ± 0.15 | 75 | $5.3 \times 10^{-5}$ |
| 7 | Oat | 37.4 | 0.004 | 4.1 | 3680 | 342 | 0.41 ± 0.11 | 77 | $5.2 \times 10^{-5}$ |
| 8 | Kinsey | 38.6 | 0.004 | 3.9 | 3300 | 357 | 0.40 ± 0.09 | 83 | $4.8 \times 10^{-5}$ |
| 9 | Big | 41.0 | 0.004 | 9.4 | 5513 | 399 | 0.58 ± 0.10 | 88 | $4.6 \times 10^{-5}$ |
| 10 | Big Flat | 45.3 | 0.004 | 16.1 | 6804 | 422 | 0.25 ± 0.14 | 121 | $3.3 \times 10^{-5}$ |
| 11 | Shipman | 47.5 | 0.004 | 8.7 | 5742 | 475 | 0.36 ± 0.09 | 108 | $3.7 \times 10^{-5}$ |
| 12 | Buck | 49.2 | 0.0033 | 3.1 | 3044 | 492 | 0.39 ± 0.08 | 109 | $3.0 \times 10^{-5}$ |
| 13 | Gitchell | 51.7 | 0.0033 | 8.4 | 5127 | 342 | 0.31 ± 0.10 | 90 | $3.7 \times 10^{-5}$ |
| 14 | Horse Mtn. | 55.0 | 0.0023 | 6.9 | 4520 | 567 | 0.47 ± 0.15 | 62 | $3.7 \times 10^{-5}$ |
| 15 | Telegraph | 56.9 | 0.001 | 7.6 | 4954 | 404 | 0.42 ± 0.14 | 60 | $1.7 \times 10^{-5}$ |
| 16 | Whale | 69.5 | 0.001 | 9.7 | 6735 | 440 | 0.37 ± 0.13 | 56 | $1.8 \times 10^{-5}$ |
| 17 | Jackass | 79.8 | 0.0005 | 13.8 | 4635 | 427 | 0.52 ± 0.13 | 45 | $1.1 \times 10^{-5}$ |
| 18 | Hardy | 100.7 | 0.0005 | 13.0 | 7202 | 470 | 0.48 ± 0.11 | 52 | $9.6 \times 10^{-4}$ |
| 19 | Juan | 101.7 | 0.0005 | 19.4 | 9810 | 397 | 0.46 ± 0.10 | 58 | $8.6 \times 10^{-4}$ |
| 20 | Howard | 104.8 | 0.0005 | 11.3 | 7038 | 482 | 0.59 ± 0.11 | 58 | $8.6 \times 10^{-4}$ |
| 21 | Dehaven | 106.5 | 0.0005 | 20.8 | 10454 | 312 | 0.36 ± 0.14 | 50 | $1.0 \times 10^{-5}$ |
| | MEAN | | 0.0012 | 11.2 | 6255 | 421 | 0.43 ± 0.22 | 71 | $3.5 \times 10^{-5}$ |

*Distance from Cape Mendocino, south along N30°W (coast-parallel) transect.

†Distance downstream from divide where drainage area is 0.1 km$^2$, corresponds to the observed scaling break between colluvial and fluvial channels (see Fig. 7).

§Main-trunk channel, 10 m contour method data (Table 3, run 1; equation 14).

vial processes. The most extensive sedimentary deposits are found behind woody-debris dams and are generally up to 50 m long and 3 m thick.

The climate of the study area is maritime and humid, with a mean annual temperature of ~13 °C. Floral evidence indicates that the temperate climate extended into the Pleistocene, without large fluctuations, such as ice-age glaciations (Johnson, 1977). Wet winters characterize the area, with 90% of the annual precipitation during the period from October to April. The orographic effect of the rugged topography of the central part of the region causes a significant variation in annual precipitation, from ~1 m north and south of the study area, to between 1.5 and 3 m in the King Range (National Weather Service data; Rantz, 1968).

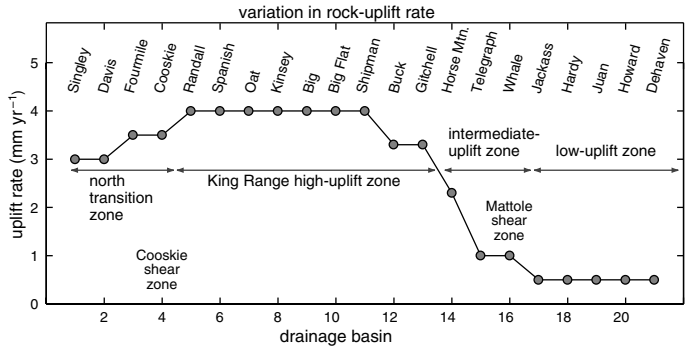


**Figure 3. Comparison of latest-Pleistocene to Holocene rock-uplift rates for the 21 study area drainage basins, from north to south. Data are from Merritts and Bull (1989).**

## EQUILIBRIUM CHANNEL HYPOTHESIS

As shown in the theoretical framework section, only longitudinal profiles of streams in equilibrium with rock uplift and prevailing climate can be interpreted directly in terms of critical model parameters (equations 13 and 14). Therefore, we need to carefully assess whether the bedrock channels in the study area are reasonably close to an equilibrium state. The question of equilibrium is most important in the high-uplift zone where channels have had only ~100 k.y. to respond to the imposed rock-uplift rate.

We expect near steady-state conditions in the low-uplift zone for two reasons. First, uplift rates in the region have been approximately constant for a long period of time, at least 330 k.y. (Merritts and Bull, 1989). Second, late Quaternary climate fluctuations have been subdued in the region (Johnson, 1977). However, our analysis implicitly concerns the time-integrated effects of climatic changes. Sea-level fluctuations likely affect sedimentation in lower reaches of the channel, but probably not the bedrock-channel reaches upstream. We make this assertion because the offshore low-gradient, wide marine bench simply would extend the length of the lower parts of the channels during sea-level lowstands, rather than dramatically affect the rate of rock uplift relative to base level. Finally, the smooth, concave longitudinal profiles, without knick zones or large-scale convexities, seen in each channel are consistent with the steady-state hypothesis. To conclude, all available indicators suggest that the low-uplift-rate streams are in or near equilibrium.

Disequilibrium conditions are more likely in the high-uplift zone because uplift rates increased only 100 k.y. ago. The shear-stress incision model predicts longitudinal profiles with a large convexity migrating upstream as a wave, and a steepened lower reach during transient response to an acceleration in uplift rate (Fig. 5). However, high-uplift-zone streams consistently exhibit smooth concave profiles without large-scale convexities. Furthermore, Merritts and Vincent (1989) showed that the high-uplift signal has already reached the first-order streams. For these reasons, we cannot disprove

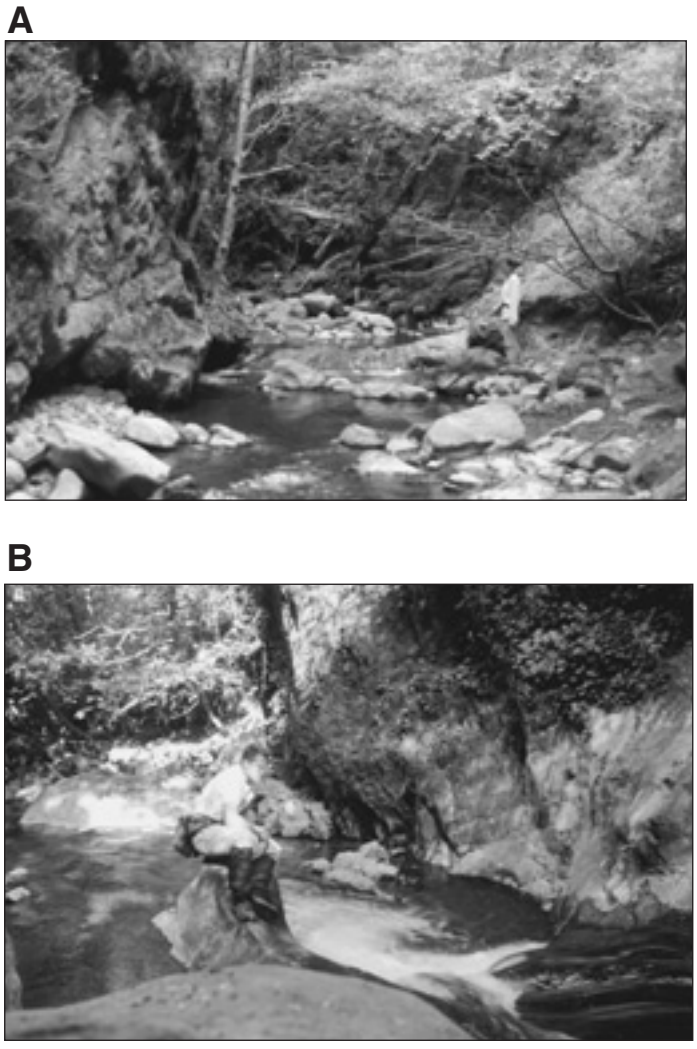


**Figure 4. Photographs of study area channel morphology. (A) A view upstream at a mixed bedrock and alluvium reach in Davis Creek; note the prominent bedrock rib across the channel. (B) Sculpted and polished bedrock in a section of relatively unjointed rocks along Shipman Creek.**

the equilibrium channel hypothesis in any of the study-area channels. Later calculations herein of response time indicate that the steady-state hypothesis is reasonable, given 100 k.y. of high-uplift-rate conditions. Our analysis proceeds by accepting the hypothesis that these channels are close to their equilibrium form.

For the observed topography to match the theory (and for the relationships of equations 13 and 14 to be valid), two criteria, in addition to steady-state erosion, must be met: both $U$ and $K$ must be spatially constant within each drainage basin. The following analysis of slope-area data assumes that these conditions exist. The observation that late Pleistocene and Holocene emergent marine terraces are not significantly tilted away from the original coastward dip supports the assumption of spatially constant uplift rate ($U$). Similarly, preliminary field observations that indicate no systematic downstream variations in either rock mass quality or the degree of sediment cover in the modeled channel reaches (defined in the following) support the assumption of spatially constant erosion coefficient ($K$). Moreover, analysis of slope-area data should detect significant downstream changes in $K$ if they occur (Slingerland et al., 1998). We proceed with the reasonable assumption that longitudinal profile analysis of the study-area channels provides direct measurements of theoretical parameters (equations 13 and 14).

## LONGITUDINAL PROFILE SLOPE-AREA ANALYSIS

### Methods

Data were acquired in three stages. First, channel longitudinal profiles (streamwise distance, elevation, and drainage area) were generated from DEMs, topographic maps, and field surveys, and the results of these methods were compared. Second, power-law regressions of channel slope as a function of drainage area were used to derive estimates of channel concavity and steepness (equation 12). This analysis was limited to include only the part of the drainage network dominated by bedrock erosion (defined in the following). Slope-area data can be generated in a variety of ways, and several methods were critically evaluated. Third, channel widths were measured in the field as a function of drainage area for two basins in the high-uplift zone.

**Channel Longitudinal Profiles.** Our analysis began with measurements of elevation and drainage area at points along the length of each study-area channel. We compared three methods of measuring channel longitudinal profiles (elevation and stream distance). The first method, field surveying (using either hand levels or inclinometers), is time consuming but accurate on a fine (<10 m) horizontal scale. Field surveys for Kinsey and Shipman Creeks were conducted (Fig. 2). The second method, digitizing elevations from topographic maps, is also laborious, with accuracy limited by the counter interval (12 m for U.S. Geological Survey [USGS] 7.5′ maps in the study area). Profiles from several channels were digitized. The third technique, extraction of channel profiles from DEMs, is highly efficient, but accuracy is limited by the resolution and quality of the DEM. In this study, USGS 30 m pixel DEMs, generated from 7.5′ topographic maps, were used. The rasterization process used to produce DEMs introduces inaccuracies on the pixel scale, and the resulting longitudinal profiles are not as smooth as those produced from the other techniques. Therefore, DEM-derived stream profiles require the implementation of some smoothing algorithm prior to computation of local slopes. DEMs are the simplest and most accurate method of generating basin-wide drainage-area data sets, and the only method used in this study for this purpose. Comparison of these three methods for several channels indicated that for the topographic analysis used in this study, the differences between the three techniques are not significant on a basin scale (Fig. 6). Therefore, the DEM-generated longitudinal profiles of all 21 channels were used for their ease in extraction and direct comparison to drainage area data (Fig. 7).

**Slope-Area Analysis.** Linear regression of the logarithms of local channel gradient and drainage area data was used to find values for the concavity index ($\theta$) and the steepness index ($k_s$) (equation 12; Fig. 7). In this section we discuss some of the complications of this type of analysis. The considerable scatter in local-slope data leads to large uncertainties in best-fit regression parameters. Much of the observed scatter in slopes can be attributed to the resolution of USGS 30 m DEMs. The results of several smoothing methods are compared.

The slope-area relations in equations 11 and 12 only have meaning in the context of detachment-limited bedrock channels, so the parts of the drainage basin where these equations are an appropriate model were isolated on the basis of inspection of the slope-area data and field observations. Regressions of slope-area data that cross process transitions do not provide useful information. The scaling break or transition between colluvial and fluvial channels has been identified from DEM data by many workers (e.g., Dietrich et al., 1993; Montgomery and Foufoula-Georgiou, 1993). For all of the

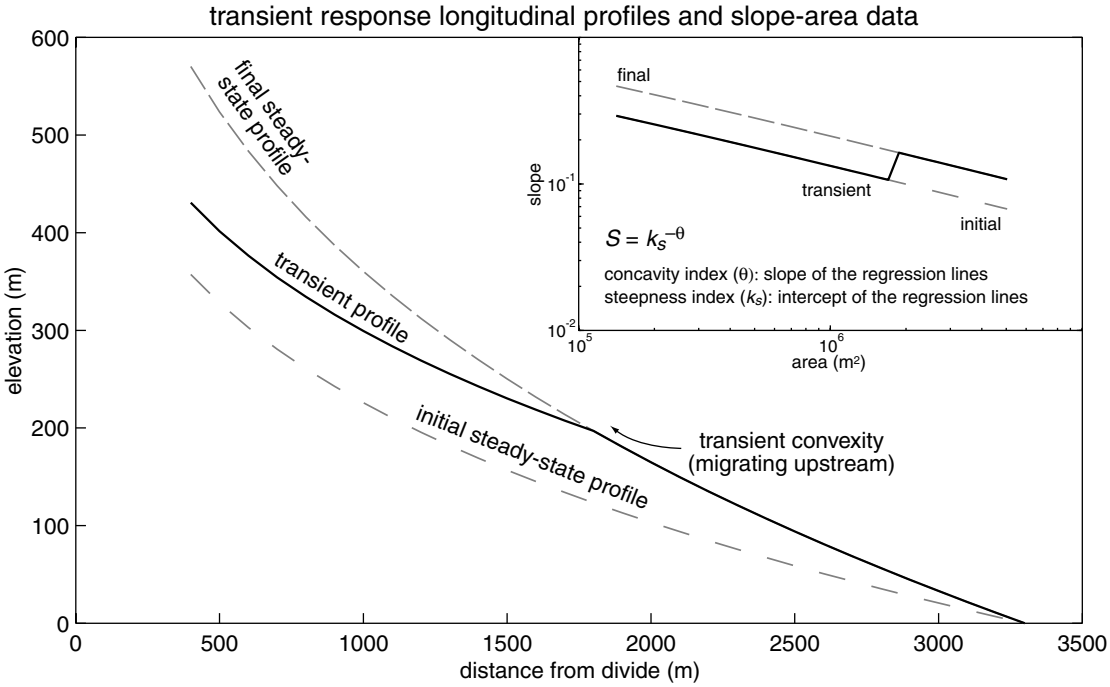


**Figure 5. Example of a simulated transient-state profile between initial low-uplift and final high-uplift zone conditions. Note the prominent convexity at the midprofile position. This knick zone migrates upstream as the channel responds to the uplift-rate change. Inset shows the slope-drainage area data for the three longitudinal profiles. Note that the channel concavity (θ, the slope of the slope-area regression line) is the same for both the initial and final profiles, while the steepness ($k_s$, the intercept) is considerably higher for the final (high uplift rate) profile.**

basins in the study area, this break is well defined and occurs at drainage areas between $10^4$ m$^2$ and $10^5$ m$^2$ (Fig. 7). Conservatively, all data points with areas $<10^5$ m$^2$ were omitted from the regression analysis. Field mapping of channel-bed characteristics indicates that the lower reaches of channels in the larger study-area basins are alluviated. The transition from bedrock to alluvial channels typically occurs at drainage areas above about $10^7$ m$^2$ and appears to be associated with a decrease in channel slope (Fig. 7). A critical drainage area of $5 \times 10^6$ m$^2$ was chosen as a conservative upper bound on bedrock channels in the regression analysis provided in the following. Limiting the data series to a defined range of drainage areas allowed for unbiased comparison between bedrock-erosion dominated channel reaches of similar size. The $10^5$ to $5 \times 10^6$ m$^2$ range in area corresponds to 3000–4000 m in horizontal channel length.

Two different sets of slope-area data were compared: those for main-trunk streams and those for entire drainage basins. First, the domain was limited to just the main channel. This technique avoided complications due to errors in computing flow paths across gently sloping terrain on ridges and valley bottoms, and reduced scatter due to interbasin variations. In addition, this method required no assumptions about tributary-channel erosion rates. Second, we used points from the entire basin (within the specified range of areas). This includes the trunk stream, as well as tributaries, and is the domain used by most previous workers (Tarboton et al., 1991; Montgomery and Foufoula-Georgiou, 1993; Tucker, 1996).

The stair-step nature of USGS 30 m DEM-derived longitudinal profiles produces considerable scatter in slope-area data, including many channel segments with zero slopes (nonphysical artifacts of DEM resolution and pit-filling routines). Therefore, some smoothing of the data was required. In order to test the sensitivity of the results to the choice of smoothing algorithm, two methods were compared. For both the basin-wide and main-channel slope-area data sets, the technique of averaging the slopes in logarithmic bins of drainage area was used, similar to other studies (Tarboton et al., 1991; Montgomery and Foufoula-Georgiou, 1993; Willgoose, 1994; Tucker and Bras, 1998). For the main-channel data sets, slopes were also calculated on interpolated 10 m contour intervals. This technique is directly analogous to measuring longitudinal profiles from topographic maps. We show the results of this comparison of methods in the next section.

**Channel-Width Measurements.** Downstream variations in channel width were measured in an attempt to constrain the *m/n* ratio (equations 4 and 9). Width data were collected for most of Kinsey Creek and the lower part of Shipman Creek. Because effective channel width is not always easy to define in rugged bedrock channels, three different width measurements were made: (1) low-flow (late summer) channel width; (2) high-flow channel width, largely defined by channel banks and vegetation patterns (roughly analogous to the bankfull condition for alluvial channels); and (3) valley-bottom width, measured from one steep side-wall to the other, commonly equal to the high-flow width in steep, narrow canyons. In general, we anticipate that the high-flow width most likely represents the geomorphically significant flow condition (Wolman and Miller, 1960). However, the valley-bottom width is also important because it is a measure of the longer term width over which the channel must operate (Pazzaglia et al., 1998). Each of these three width measurements varied considerably on the 10 m scale along the channel. Therefore, a large number of measurements were made to characterize the overall increase in channel width with drainage area. Measurements were taken at regular intervals, spaced ~50 m apart along the stream profile.

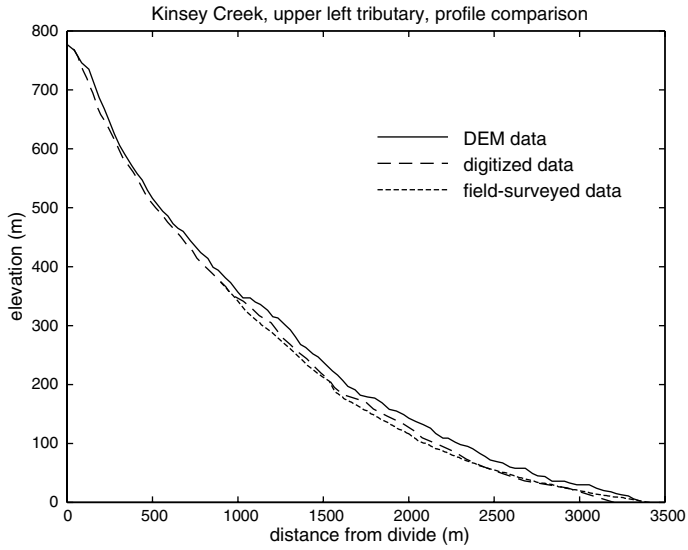


**Figure 6. Comparison of longitudinal profiles for Kinsey Creek, upper left tributary. An ~4× vertical exaggeration is used to highlight differences. Outlet of each profile is arbitrary, and no effort has been made to match this point. The surveyed profile did not reach the divide, and was done using both hand level and hand inclinometer. Slope-area regressions of the two complete profiles (digital elevation model [DEM] and digitized) yield values of θ and $k_s$ (equation 12) that are indistinguishable from each other.**

## Results

**Comparison of Slope-Area Techniques.** In general, the three different slope-area methods produce similar values of θ, and similar correlations between $k_s$ and $U$, from regression analyses of equation 12 (Table 2). The two calculations that use only the main channel data points produce nearly identical results (methods 1 and 2). The calculation using the basin-wide data set produces a slightly higher mean value for θ. We use the method 1 data (main-trunk channel, elevation-contoured slopes) for subsequent discussion and calculations. This technique is the simplest and least subject to error or unintended bias, for four reasons: (1) by using only the main-channel data, we need not make any assumptions about the response of small, steep side-slope tributaries; (2) by averaging slopes on 10 m contours we give each elevation interval within the profile equal weight in the regression; (3) the 10 m contouring method averages out much of the noise introduced by the poor vertical resolution of USGS 30 m DEMs (particularly in steep, narrow basins); and (4) the contour method is directly comparable to profiles digitized from topographic maps.

**Channel Width to Drainage-Area Relation.** Our preliminary measurements of the power-law relationship between channel width and drainage area, based on equation 4, are presented in Table 3. The data for Kinsey Creek span a full order of magnitude in drainage area, and therefore are constrained much better than for Shipman Creek. As noted earlier, empirical data for small basins with alluvial channels ($b \sim 0.5$, $c \sim 1$) predicts that channel width will increase with the square root of drainage area. In Kinsey Creek, the high-flow and valley-bottom widths increase with drainage area to the 0.6– 0.7 power ($bc$, equation 4; Table 4), higher than the expected relation for alluvial channels. Assuming that discharge increases approximately linearly with drainage area ($c = 1$), then $b$ is likely to be greater than 0.5. For the purposes of calculations in the rest of this paper we use $b = 0.6$ and $c = 1$. Using these estimates, the shear-stress incision model predicts that the $m/n$ ratio for these streams should be 0.4 (equation 9).

**Measurements of Channel Concavity.** The values of the concavity index (θ) for 17 of the 21 channels agree within 2σ errors (equations 11 and 12, Fig. 8 and Table 1). The individual measurements of θ range from 0.25 to 0.59, and produce an error-weighted mean value of 0.43 ± 0.22 (2σ). This mean value (and range of values) is similar to other slope-area analyses (Hack, 1957; Flint, 1974; Tarboton et al., 1991; Moglen and Bras, 1995; Slingerland et al., 1998). The scatter in the slope-area data is considerable, as are the uncertainties on estimated θ values. However, the mean value is consistent with both the theoretical prediction that $m/n$ should depend only on the exponents $b$ and $c$ (equations 9 and 13) (Whipple and Tucker, 1999) and the equilibrium channel hypothesis. The approximately constant concavity index (θ) of 0.43 throughout the study area agrees well with the expected value of 0.4 (equation 9). We consider the mean value of θ a good representation of the study-area channel concavity, to be used in subsequent calculations, because the data reveal no systematic, statistically significant deviations from the mean as a function of rock-uplift rate. The good agreement between the concavity results from all three slope-area methods further supports this assertion and indicates that the mean value is not dependent on technique (Table 2).

**Measurements of Channel Steepness.** To facilitate direct comparison among the drainage basins, we calculate the steepness index ($k_s$) for the mean value of θ = 0.43 for all 21 channels (equations 11 and 12; Fig. 8 and Table 1). This is necessary because small changes in θ produce large apparent changes in $k_s$. Given that few of the regressions produce statistically significant differences in θ away from the mean value of 0.43, such apparent variations in $k_s$ likely reflect only the inherent scatter in slope-area data. Fixing the profile concavity to standardize the calculation of profile steepness is directly analogous to measuring deviations from an assumed logarithmic profile form in the stream-gradient index technique (Hack, 1973; Merritts and Vincent, 1989; Goldrick and Bishop, 1995) and the normalization technique described by Sklar and Dietrich (1998).

The steepness values thus derived broadly correlate to the uplift-rate data, with above-average values in the high-uplift zone (drainage basins 5–13) and below-average values in the low-uplift zone (drainage basins 17–21; Fig. 8). The relation between uplift and steepness is expected, because steepness is essentially a measure of the ratio of basin relief and basin length, which is much higher in the rugged high-uplift zone. This relationship was also observed in the channel-reach-slope analysis by Merritts and Vincent (1989). The two populations can be averaged to produce representative steepness indices of 92 in the high-uplift zone and 53 in the low-uplift zone (Table 2). Via the equilibrium channel hypothesis (equations 13 and 14), these rough values allow for some simple calculations to constrain the coefficient of erosion ($K$), the slope exponent ($n$), and basin-response time scale.

## DISCUSSION

### Implications of Constant Channel Concavity

This study shows that concavity is generally constant within measurement error among the 21 drainage basins. This observation is consistent with a prediction of the shear-stress incision model (equations 9 and 13; Whipple and Tucker, 1999), and has important implications for possible downstream variation of the erosion coefficient, and the style of channel response to changes in uplift rate.

As mentioned previously, if $K$ significantly changes downstream within a basin as a function of sediment load (Sklar and Dietrich, 1998), we would expect to see differences in channel concavity within a profile from that expected for the simple shear-stress model. Because the profiles exhibit

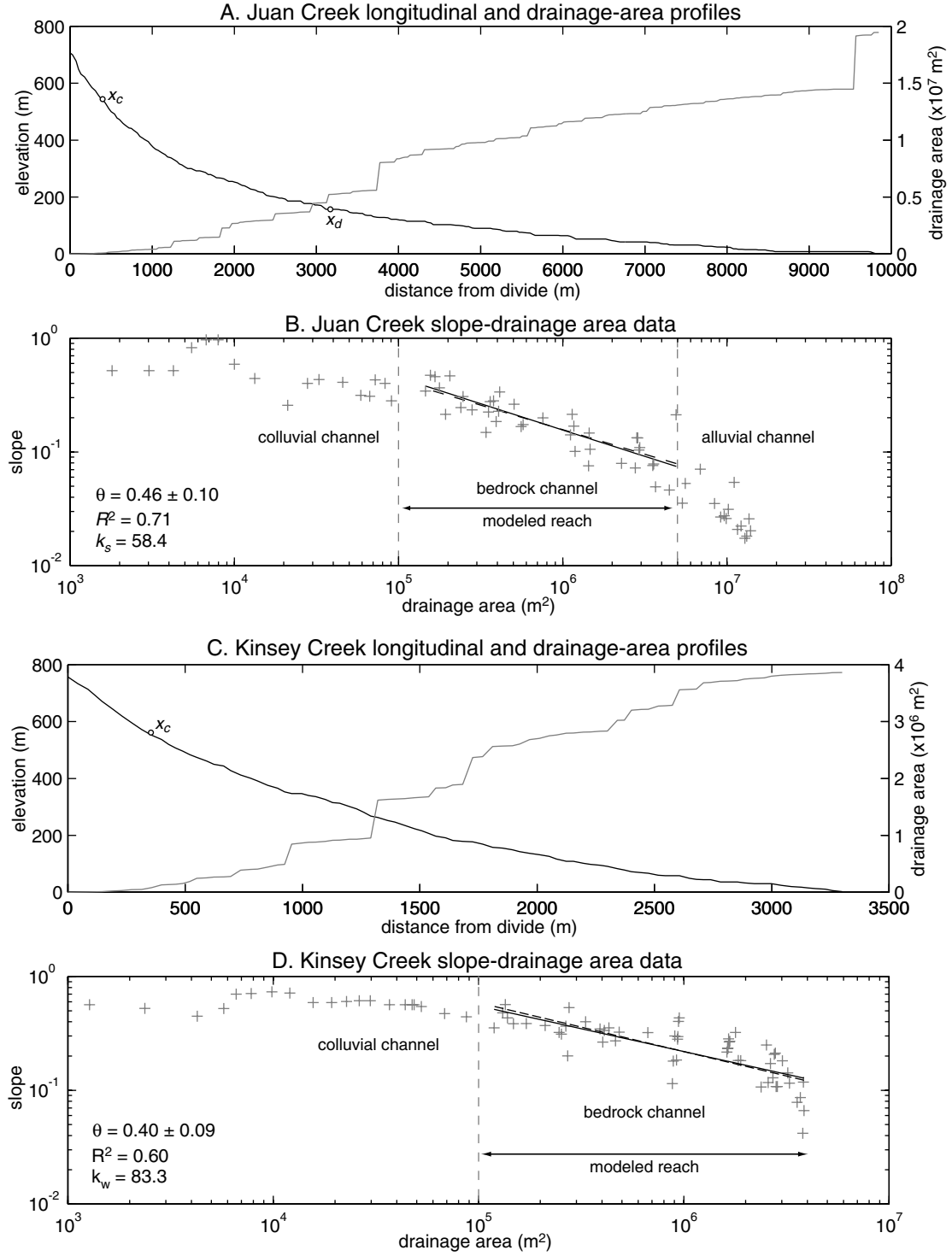


**Figure 7. Examples of digital elevation model–derived channel topographic data from Juan Creek, in the low-uplift-rate zone, and Kinsey Creek, in the King Range high-uplift-rate zone. Note that the scales are different for the two streams. (A, C) Longitudinal profile (black line) and drainage area profile (gray line); steps correspond to tributary junctions. For Juan Creek, the bedrock-channel study domain is between $x_c$ (drainage area, $A = 10^5$ m$^2$) and $x_d$ ($A = 5 \times 10^6$ m$^2$). Kinsey Creek is smaller than the $A = 5 \times 10^6$ m$^2$ threshold, so the entire channel below $x_c$ is within the study domain. (B, D) Slope and drainage-area data with regression lines. Data domain in these examples only includes the main channel, with slopes calculated for 10 m elevation intervals. From equation 12, the slope of these lines is θ and the y-axis intercept is $k_s$. Solid line is the least-squares best fit, used to calculate θ. Dashed line is the best fit with θ = 0.43 used to calculate $k_s$. If the regression domain for Juan Creek includes drainage areas greater than $5 \times 10^6$ m$^2$, then θ = 0.60 ± 0.07. This greater concavity is seen in all of the low-uplift drainages if the lower, alluvial part of the channel is included in the regression domain.**

TABLE 2. COMPARISON OF SLOPE-AREA METHODS

| No. | Slope domain | Slope calculation method | θ mean ± 1σ | $k_s$ mean ± 1σ* | $k_s$ mean ± 1σ* | |
|---|---|---|---|---|---|---|
| | | | | | High-uplift | Low-uplift |
| 1 | Main-trunk channel | 10 m elevation contours | 0.43 ± 0.11 | 71 ± 22 | 92 ± 17 | 53 ± 6 |
| 2 | Main-trunk channel | log-bin average | 0.44 ± 0.14 | 73 ± 21 | 93 ± 17 | 55 ± 6 |
| 3 | Entire basin | log-bin average | 0.46 ± 0.09 | 98 ± 30 | 129 ± 17 | 66 ± 4 |

*Calculated with θ = θ mean.

smooth, uniform concavities consistent with those expected from theory and preliminary width-area data, we see no evidence for downstream changes in $K$ over the modeled reaches ($10^5$ m$^2 \le A \le 5 \times 10^6$ m$^2$). This observation is congruent with the finding of Slingerland et al. (1998) that channel-profile concavities in the Central Range of Taiwan are more consistent with a shear-stress or unit-stream-power incision rule than with a sediment-flux–dependent erosion rule. However, the relatively short length of channels studied here may prevent detection of the effects of a gradual downstream increase in $K$. Further research of this issue is warranted.

## Channel Response to Tectonic Forcing

We now explore constraints on two key unknowns ($K$ and $n$) in the shear-stress incision model (equation 5) by comparing stream-profile data of the high- and low-uplift zones. Under the equilibrium channel hypothesis, equation 14 is valid, and since $U$ is known, some broad constraints can be placed on both the slope exponent ($n$) and possible dynamic adjustment of the coefficient of erosion ($K$) in response to changes in uplift rate. Naturally, the analysis that follows depends on both the accuracy of the uplift-rate data and the estimated steepness index ($k_s$) values (Table 2). The effects of the variation in tectonic conditions within the study area are shown by solving equation 14 for $K$ and dividing the high-uplift-rate case (subscript 2) by the low-uplift-rate case (subscript 1):

$$K_2/K_1 = (U_2/U_1)(k_{s1}/k_{s2})^n. \quad (15)$$

This equation allows us to analyze the magnitude of possible changes in the value of $K$ between the different uplift-rate zones, given broad theoretical constraints on the plausible range of the slope exponent ($n$) (Foley, 1980; Howard and Kerby, 1983; Howard et al., 1994; Hancock et al., 1998; Whipple et al., 2000). Implicit in this approach is the assumption that erosion process (and therefore $n$) does not change with uplift rate.

In landscape-evolution models that consider zones of similar climate and lithology, $K$ often is assumed to be a constant throughout the model domain. This assumption is testable by setting $K$ constant throughout the study area ($K_2/K_1 = 1$), and solving equation 15 for $n$. A simple calculation using $k_{s1} = 53$ and $k_{s2} = 92$ (the low- and high-uplift zone mean values, respectively) indicates that for $K$ to be constant throughout the study area, $n$ must be 3.8 (Fig. 9A). If we set $k_{s2} = 74$ and 121 (the minimum and maximum high-uplift zone values, respectively) then $n$ must be 6.2 and 2.5, respectively. These values are considerably higher than any suggested by theoretical arguments (Foley, 1980; Howard and Kerby, 1983; Howard et al., 1994; Hancock et al., 1998; Whipple et al., 2000), suggesting that $K$ is probably greater in the high-uplift zone than the low-uplift zone (Fig. 9A). Given the likely range of $n$ values, $K$ must increase two to six fold between the low- and high-uplift zones. For example, with $n$ equal to 1 (a commonly cited value, with $a = 3/2$), equation 15 indicates at least a four- to five-fold variation in $K$ (Fig. 9A), with mean values for the low- and high-uplift zones of $9.6 \times 10^{-6}$ and $4.4 \times 10^{-5}$ m$^{0.14}$ yr$^{-1}$ (units calculated with $m = n\,\theta$, from equation 13), respectively (Fig. 8; Table 1). This change in erosion coefficient corresponds to an eight-fold variation in uplift rate; high $K$ values are associated with the high-uplift zone. We now have two end-member cases: either $n$ is quite large and $K$ is constant throughout the study area, or $n \sim 1$ and $K$ varies significantly between the high- and low-uplift zones. Such dynamic adjustment of $K$ is not unexpected given present knowledge of the geomorphic controls on bedrock-incision rates.

Variations in lithology will directly affect the value of the erosion-rate coefficient. The rocks of the study area range from mudstones to sandstones. The King Range terrane is mapped as more argillaceous than sandstone rich, while in the low-uplift zone sandstone predominates over finer grained sedimentary rocks (McLaughlin et al., 1994). However, preliminary field measurements of intact rock strength (using a Schmidt Hammer), joint spacing, and weathering characteristics by the authors, and detailed aerial-photograph analysis of hillslope morphology by S. Ellen (unpublished data) do not reveal any systematic large-scale variations in lithologic resistance. More work is necessary before a lithologic explanation can be ruled out with certainty, but at present north to south changes in lithology appear unimportant. The data for Cooskie Creek provide an important exception (Fig. 8, drainage 4). This basin is oriented along a shear zone and was previously identified as a zone of weaker lithology (Beutner et al., 1980; McLaughlin et al., 1994). It is interesting that this drainage has the highest value of $K$ in the study area, indicating that this methodology can indeed detect differences in bedrock resistance.

Increased orographic precipitation in the King Range high-uplift zone, where a maximum three-fold increase in annual precipitation is observed (Rantz, 1968), is one known source of variation in $K$. This change in precipitation will most likely directly affect the value of $k_q$, the coefficient as-

TABLE 3. CHANNEL WIDTH AND DRAINAGE AREA RELATIONSHIP

| Drainage basin | Width measurement | Drainage area range (m$^2$) | $bc$ (± 2σ)* | $k_w k_q^b$ | Number of data points |
|---|---|---|---|---|---|
| Kinsey Creek | Low flow | $3 \times 10^5 - 3.9 \times 10^6$ | 0.43 ± 0.13 | $6.9 \times 10^{-3}$ | 50 |
| | High flow | $3 \times 10^5 - 3.9 \times 10^6$ | 0.65 ± 0.19 | $6.9 \times 10^{-4}$ | 48 |
| | Valley bottom | $3 \times 10^5 - 3.9 \times 10^6$ | 0.67 ± 0.23 | $5.5 \times 10^{-4}$ | 39 |
| Shipman Creek | Low flow | $3 \times 10^6 - 8.7 \times 10^6$ | 0.61 ± 0.33 | $5.5 \times 10^{-4}$ | 50 |
| | High flow | $3 \times 10^6 - 8.7 \times 10^6$ | 0.46 ± 0.32 | $9.4 \times 10^{-3}$ | 49 |
| | Valley bottom | $3 \times 10^6 - 8.7 \times 10^6$ | 0.50 ± 0.47 | $6.6 \times 10^{-3}$ | 49 |

*Power-law model based equation 4: $W = (k_w k_q^b) A^{bc}$.

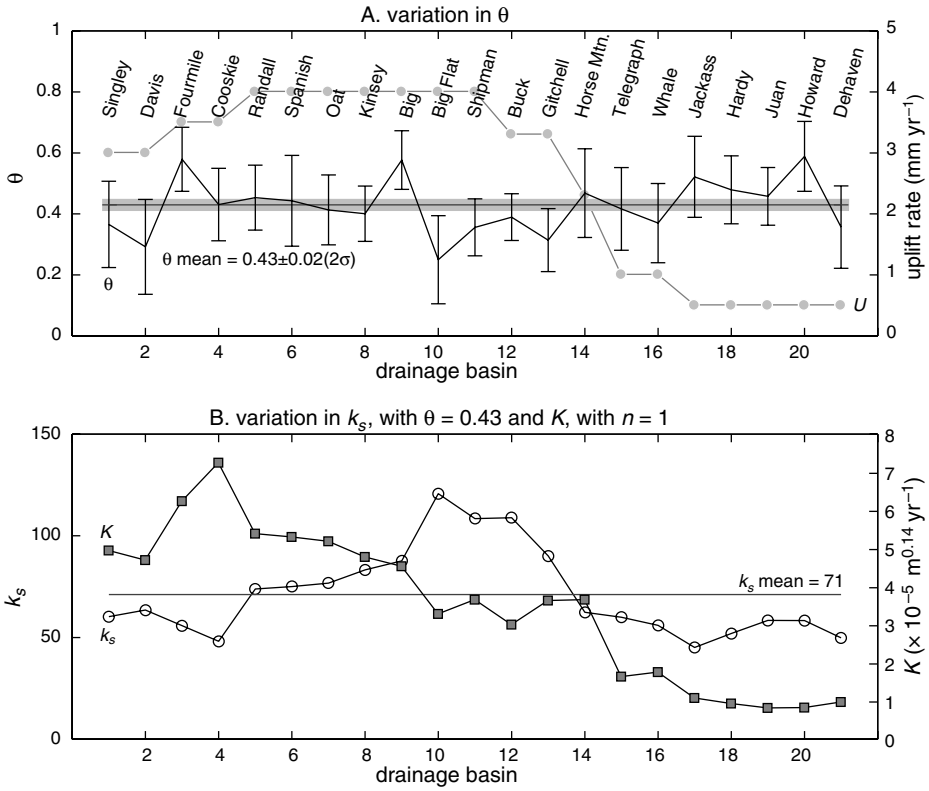


**Figure 8. Comparisons among the 21 study-area channels, from north to south. (A) Concavity index (θ, with error bars) calculated from slope-area data using the equation 12 relation. Error bars show 2σ uncertainty on each regression. Shaded area represents the mean value with 2σ error on its calculation, as opposed to the error-weighted mean value cited in the text. Also included is the uplift-rate graph from Figure 3. (B) Steepness index ($k_s$, circles) calculated from equation 12 with θ = 0.43 and erosion coefficient ($K$, squares) calculated from equation 14 with $n$ = 1.**

sociated with the discharge-area relation (equation 3). Because we have no specific information about the change in flood magnitudes and frequencies, we make the simplifying assumption that the dominant discharge is proportional to mean-annual precipitation. To explore this aspect of the erosion coefficient, we isolate contribution of enhanced runoff on the value of $K$ by using equations 6 and 8:

$$K = K' k_q^{n(1-b)}, \tag{16}$$

where $K'$ is controlled by substrate lithology, sediment flux, and channel width. Substituting equation 16 into equation 15 and solving for the remaining variation in the coefficient of erosion ($K_2'/K_1'$) yields

$$\frac{K_2'}{K_1'} = \left(\frac{U_2}{U_1}\right)\left[\left(\frac{k_{s1}}{k_{s2}}\right)\left(\frac{k_{q1}}{k_{q2}}\right)^{(1-b)}\right]^n, \tag{17}$$

where the ratio $k_{q1}/k_{q2} \sim 1/3$ (Rantz, 1968). With $b = 0.6$ and the same $k_{s1}$ and $k_{s2}$ values as above, the $n = 1$ case yields a two- to four-fold variation in $K'$ between the high- and low-uplift zones (Fig. 9B). Alternatively, we can make the simplifying (but probably incorrect) assumption that $K$ varies solely and directly in response to this precipitation difference ($K_2'/K_1' = 1$), and solve equation 17 for $n$. This calculation gives an average value for $n$ of 2.1, with a range of 1.6 to 2.7. These values of $n$ just overlap with the range of those suggested by theoretical considerations ($n \sim 2/3$ to 5/3; Fig. 9B). Therefore, precipitation differences can explain some, and perhaps all, of the variation in $K$. However, as shown in Figure 9B, for most of the range of plausible n values, $K$ must increase by a factor of 1.5 to 4.5 beyond that attributable to orographic precipitation. Moreover, several other factors that influence $K$ are likely to change in response to increased rates of rock uplift.

As mentioned earlier, holding $K$ constant carries with it the implicit assumption that only channel slope is free to adjust to changes in boundary conditions. At least four other channel attributes that influence $K$ may adjust in concert with channel slope: channel width, amount of alluvial cover, sediment flux, and frequency of debris flows. First, channels are likely to narrow in response to the steepening caused by increased uplift rates. Second, the degree of alluvial cover may also be an important control on $K$. Sediment can protect the bed, reducing or stopping erosion (Sklar and Dietrich, 1998). Third, increased sediment flux may increase the erosivity of floods. Fourth, the increased steepness and orographic precipitation associated with higher uplift rates may produce an increase in the frequency of debris-flow events. This might result in more erosive conditions and a higher effective value for $K$, although a complete transition to debris-flow dominated conditions might be expected to invalidate the assumptions of the shear-stress model (Stock and Dietrich, 1998).

Although we cannot at present solve for a unique combination of $K$ and $n$ for this field area, our analysis does place some constraints on these parameters. The most likely case, based on our present knowledge, is that $K$ varies systematically between the high- and low-uplift zones and that $n$ is less than 2. The finding that $K$ (and perhaps $n$) changes significantly depending on boundary conditions implies that a fully generalized shear-stress model will require similar studies in a variety of geologic, tectonic, and lithologic conditions in order to quantify these effects.

### Time Scale of Response Calculations

The King Range provides an excellent setting to explore the time scale of basin response to a change in tectonic conditions. Around 100 ka, uplift rates in the high-uplift zone accelerated from 0.5–1.2 mm yr$^{-1}$ to 4 mm yr$^{-1}$ (Merritts and Bull, 1989). We have proposed that the trunk streams have achieved steady state in response to this change, and we test whether this hy-

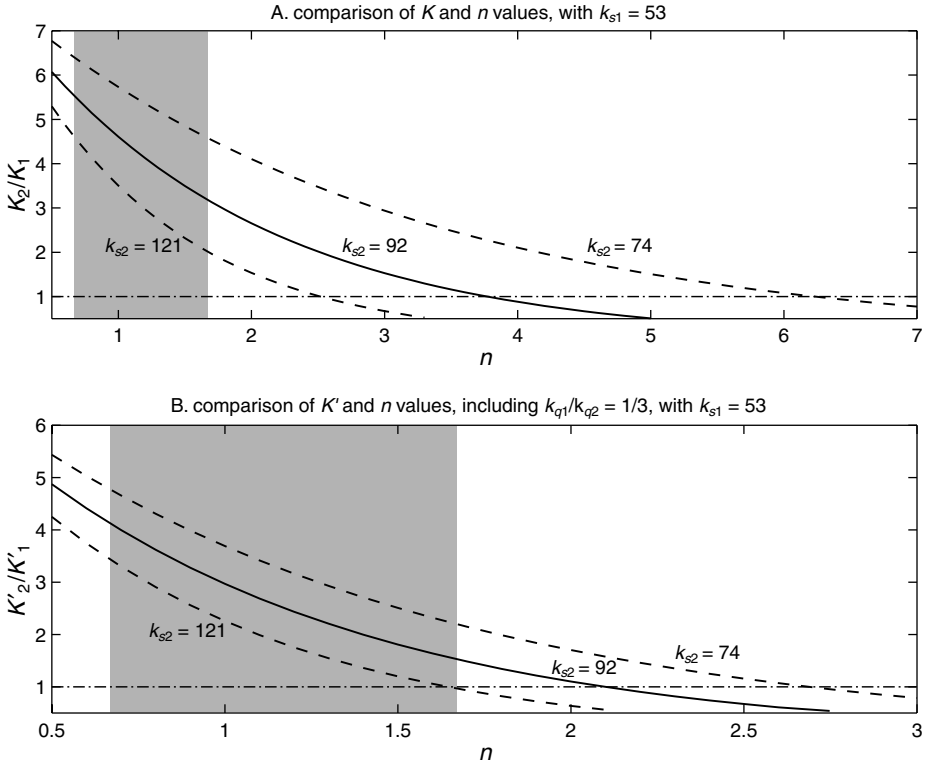


**Figure 9. Calculations of erosion coefficient (*K*) and slope exponent (*n*). (A) The ratio of high-uplift-rate to low-uplift-rate erosion coefficients ($K_2/K_1$) calculated for values of *n* from 0.5 to 7, using equation 15, with uplift rates, $U_1$ = 0.0005 m yr$^{-1}$ and $U_2$ = 0.004 m yr$^{-1}$, and steepness index, $k_{s1}$ = 53. Shaded region indicates region of theoretically predicted values of *n*. Solid line is the mean value of $k_{s2}$, dashed lines are for the minimum and maximum. This calculation indicates that n must be greater than 2.5 for *K* to be constant throughout the study area, or that *K* varies widely. (B) The same calculation as in A, but now taking into account the observed variation in orographic precipitation, using equation 17, with the *U* and $k_s$ values as above, and *b* = 0.6. This calculation suggests that if and only if *n* ~ 2, *K* varies directly and solely with discharge (or precipitation) differences. For most of the expected range of *n* values these data suggest that *K* increased by a factor of 1.5 to 4.5 beyond that expected from orographic effects in response to the eight-fold increase in uplift rate.**

pothesis is internally consistent with the shear-stress model via the following analysis. Whipple and Tucker (1999) derived the response time (defined as the time required to attain a new steady-state condition) for a change in uplift rate ($T_U$). Their analysis explicitly assumed that *K* remains constant during landscape response. Here we generalize their result by writing their equation 34 in dimensional form and allowing for the possibility that *K* adjusts in concert with incision rate:

$$T_U = \frac{k_a^{\frac{m}{n}}\left(1-\frac{hm}{n}\right)^{-1} K_f^{-\frac{1}{n}} U_f^{\frac{1}{n}-1}\left(L^{1-\frac{hm}{n}} - x_c^{1-\frac{hm}{n}}\right)\left[1-\left(\frac{K_i}{K_f}\right)^{-\frac{1}{n}}\left(\frac{U_i}{U_f}\right)^{\frac{1}{n}}\right]}{\left(1-\frac{U_i}{U_f}\right)}, \quad (18)$$

where $x_c$ is the critical distance downslope from the divide to the top of the fluvial channel network ($A = 10^5$ m$^2$), *L* is the basin length (Table 1), $k_a$ and *h* relate drainage area to channel distance ($A = k_a x^h$, where *x* denotes horizontal channel distance; Hack, 1957), and the subscripts *i* and *f* refer to initial and final conditions, respectively. The derivation of equation 18 assumes that *K* only changes below the upstream propagating wave of incision (i.e., downstream of the convexity in Fig. 5). We use equation 14 to rewrite equation 18 in a simpler form in terms of $k_{si}$ and $k_{sf}$:

$$T_U = \frac{k_a^{\frac{m}{n}}\left(1-\frac{hm}{n}\right)^{-1} \frac{k_{sf}}{U_f}\left(L^{1-\frac{hm}{n}} - x_c^{1-\frac{hm}{n}}\right)\left[1-\frac{k_{si}}{k_{sf}}\right]}{\left(1-\frac{U_i}{U_f}\right)}, \quad (19)$$

showing that, in this case, the response time scale can be evaluated without knowledge of *n*. Equation 19 is implemented by assembling 3 pieces of data for each of the 9 high-uplift drainage basins: (1) the channel characteristics from Table 1; (2) an empirical drainage-area to stream-distance relationship (Hack, 1957); and (3) an assumed initial low-uplift condition ($U_i$ = 0.5 mm yr$^{-1}$, $k_{si} = k_{s1}$ = 53) with the present-day drainage-network structure (drainage area and distance along trunk streams). With these parameters, we generate modeled initial and final steady-state profiles and solve for the time scale of response between them (Fig. 10). This calculation yields response times from 47.4 k.y. to 196 k.y., with a mean of 102 k.y. Five of the nine channels have calculated response times of ~100 k.y. or less, indicating that the steady-state assumption is reasonable. This analysis suggests that bedrock channels, at least in small basins with weak lithology, have a remarkable ability to respond rapidly to changes in tectonic forcing. Equation 18 indicates explicitly that an increase in *K* resulting from channel morphologic adjustments to an increase in uplift rate ($K_i/K_f < 1$) accelerates response time, underscoring the importance of the dynamic adjustment of the coefficient of erosion to the tectonic response of the landscape.

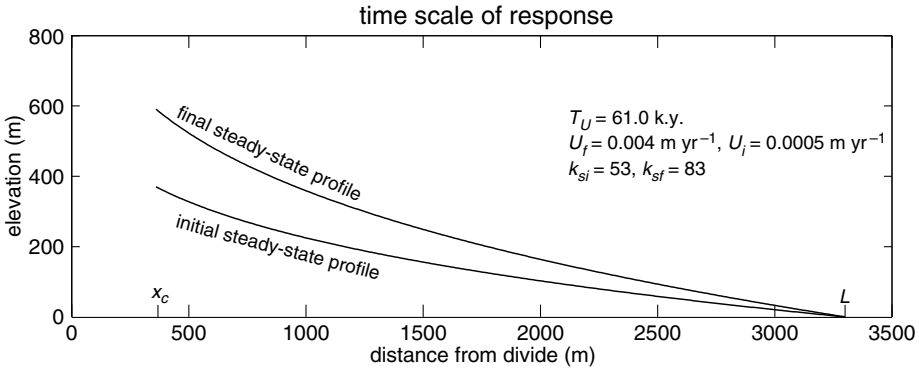


**Figure 10. An example of a time scale of response ($T_U$) calculation using equation 19. Model stream-profile parameters are from Kinsey Creek, in the high-uplift zone.**

## CONCLUSIONS

This study of field and DEM data from streams in the variable rock-uplift-rate Mendocino triple junction region produces three important outcomes with implications for the shear-stress model of bedrock-channel incision, and landscape evolution in general. (1) The main channels have uniform concavity regardless of uplift rate; (2) the erosion coefficient is not a constant, but varies in concert with rock-uplift rate; and (3) the streams appear to respond rapidly to tectonic forcing, at a rate that appears to be internally consistent with the model.

The DEM slope-area analysis of longitudinal profiles yields the important result that within uncertainty, the concavity index ($\theta$ or $m/n$ via the equilibrium hypothesis, equation 13) does not vary throughout the study area (Fig. 8). This observation is consistent with shear-stress incision model predictions (Whipple and Tucker, 1999), and the mean value ($\theta = 0.43 \approx m/n$) is broadly consistent with preliminary observations of channel width (equations 4 and 9). In addition, channel steepness correlates ($k_s$) well with uplift rate, supporting the method.

The parameters from the slope-area analysis place constraints on possible values of the key unknowns in the shear-stress model, the erosion coefficient ($K$) and the slope exponent ($n$, equations 13 and 14). In particular, $K$ appears to have adjusted to tectonic conditions. Since the problem involves one equation with two unknowns, values between two end-member cases, either a constant $K$ or $n = 1$, are explored. These two cases yield the result that either: (1) $K$ is constant and $n$ is greater than 2.5, or (2) $K$ varies with uplift rate, exhibiting a five-fold increase if $n$ is assumed to be unity (Fig. 9A). If $K$ is allowed to vary directly with orographic precipitation, then models with $n \sim 2$ satisfactorily explain observed channel steepness ($k_s$) values (Fig. 9B). While theoretical formulations allow values of the slope exponent ($n$) up to ~2 (Foley, 1980; Hancock et al., 1998; Whipple et al., 2000), changes in channel width, sediment load, and debris-flow frequency are likely to influence $K$. These calculations strongly support the hypothesis that the erosivity of bedrock channels dynamically adjusts to imposed tectonic conditions, illustrating an important feedback between evolution of topography and the mechanisms of channel incision: as the mountains rise, erosion becomes more effective. This preliminary evidence for dynamic adjustment highlights the need for further study of the roles of channel narrowing, changing erosion processes, and changing sediment load as response mechanisms in bedrock channels. We caution that the degree of dynamic adjustment of $K$ may be strongly dependent on lithologic, tectonic, and climatic conditions.

The King Range high-uplift zone channels support the observation, made in other orogens, that rivers have a remarkable ability to keep pace with tectonic base-level forcing (e.g., Burbank et al., 1996). The studied channels appear to have achieved a new steady state in response to an eightfold change in uplift rate in ~100 k.y., a result supported by observations of longitudinal profiles and a simple calculation of response time. This rapid response likely results from dynamic adjustment of factors controlling bedrock-incision rate, including increased precipitation, and possibly changes in channel width, sediment load, and debris-flow frequency. These complicated responses to changes in boundary conditions underscore the need for future work in other areas to generalize the shear-stress incision model.

## ACKNOWLEDGMENTS

This research was funded by National Science Foundation grants EAR-9725723 to Whipple and EAR-9725348 to Merritts. We thank Jason Nicholas, Erin Carlson, Emily Himmelstoss, and Simon Brocklehurst for field assistance, Steve Ellen for aerial-photograph analysis, and Jeff Niemann for discussions that helped motivate our interest in returning to the Mendocino triple junction area. The manuscript benefited greatly from thorough reviews by David Montgomery, Frank Pazzaglia, and Ellen Wohl.

### REFERENCES CITED

Anderson, R.S., 1994, The growth and decay of the Santa Cruz Mountains: Journal of Geophysical Research, v. 99, p. 20161–20180.

Beaumont, C., Fullsack, P., and Hamilton, J., 1992, Erosional control of active compressional orogens, *in* McClay, K.R., ed., Thrust tectonics: London, Chapman and Hall, p. 1–18.

Beutner, E.C., McLaughlin, R.J., Ohlin, H.N., and Sorg, D.H., 1980, Geologic map of the King Range and Chemise Mountain instant study areas, northern California: U.S. Geological Survey, scale 1:62 500.

Burbank, D.W., Leland, J., Fielding, E., Anderson, R.S., Brozovic, N., Reid, M.R., and Duncan, C., 1996, Bedrock incision, rock uplift and threshold hillslopes in the northwestern Himalayas: Nature, v. 379, p. 505–510.

Dietrich, W.E., Wilson, C.J., Montgomery, D.R., and McKean, J., 1993, Analysis of erosion thresholds, channel networks, and landscape morphology using a digital terrain model: Journal of Geology, v. 101, p. 259–278.

Dunne, T., and Leopold, L.B., 1978, Water in environmental planning: New York, W.H. Freeman and Company, 818 p.

Flint, J.J., 1974, Stream gradient as a function of order, magnitude, and discharge: Water Resources Research, v. 10, p. 969–973.

Foley, M.G., 1980, Bedrock incision by streams: Geological Society of America Bulletin, Part II, v. 91, p. 2189–2213.

Goldrick, G., and Bishop, P., 1995, Differentiating the roles of lithology and uplift in the steepening of bedrock river long profiles: An example from southeastern Australia: Journal of Geology, v. 103, p. 227–231.

Hack, J.T., 1957, Studies of longitudinal stream profiles in Virginia and Maryland: U.S. Geological Survey Professional Paper 294-B, p. 42–97.

Hack, J.T., 1973, Stream profile analysis and stream-gradient index: U.S. Geological Survey Journal of Research, v. 1, p. 421–429.

Hancock, G.S., Anderson, R.S., and Whipple, K.X., 1998, Beyond power: Bedrock incision process and form, *in* Tinkler, K.J., and Wohl, E.E., eds., Rivers over rock: Fluvial processes in bedrock channels: American Geophysical Union Geophysical Monograph 107, p. 35–60.

Hoffman, P.F., and Grotzinger, J.P., 1993, Orographic precipitation, erosional unloading, and tectonic style: Geology, v. 21, p. 195–198.

Howard, A.D., 1994, A detachment-limited model of drainage basin evolution: Water Resources Research, v. 30, p. 2261–2285.
Howard, A.D., 1998, Long profile development of bedrock channels: Interaction of weathering, mass wasting, bed erosion, and sediment transport, *in* Tinkler, K.J., and Wohl, E.E., eds., Rivers over rock: Fluvial processes in bedrock channels: American Geophysical Union Geophysical Monograph 107, p. 297–320.
Howard, A.D., and Kerby, G., 1983, Channel changes in badlands: Geological Society of America Bulletin, v. 94, p. 739–752.
Howard, A.D., Seidl, M.A., and Dietrich, W.E., 1994, Modeling fluvial erosion on regional to continental scales: Journal of Geophysical Research, v. 99, p. 13971–13986.
Johnson, D.L., 1977, The late Quaternary climate of coastal California: Evidence for an ice age refugium: Quaternary Research, v. 8, p. 154–179.
Kooi, H., and Beaumont, C., 1996, Large-scale geomorphology: classical concepts reconciled and integrated with contemporary ideas via a surface processes model: Journal of Geophysical Research, v. 101, no. B2, p. 3361–3386.
Koons, P.O., 1995, Modeling the topographic evolution of collisional belts: Annual Reviews of Earth and Planetary Science, v. 23, p. 375–408.
Leopold, L.B., and Miller, J.P., 1956, Ephemeral streams—Hydraulic factors and their relation to the drainage net: U.S. Geological Survey Professional Paper 282A, p. 1–37.
McLaughlin, R.J., Lajoie, K.R., Sorg, D.H., Morrison, S.D., and Wolfe, J.A., 1983, Tectonic uplift of a middle Wisconsin marine platform near the Mendocino triple junction, California: Geology, v. 11, p. 35–39.
McLaughlin, R.J., Sliter, W.V., Frederiksen, N.O., Harbert, W.P., and McCulloch, D.S., 1994, Plate motions recorded in tectonostratigraphic terranes of the Franciscan complex and evolution of the Mendocino triple junction, northwestern California: U.S. Geological Survey Bulletin 1997, 60 p.
Merritts, D.J., 1996, The Mendocino triple junction: Active faults, episodic coastal emergence, and rapid uplift: Journal of Geophysical Research, v. 101, no. B3, p. 6051–6070.
Merritts, D., and Bull, W.B., 1989, Interpreting Quaternary uplift rates at the Mendocino triple junction, northern California, from uplifted marine terraces: Geology, v. 17, p. 1020–1024.
Merritts, D., and Ellis, M., 1994, Introduction to special section on tectonics and topography: Journal of Geophysical Research, v. 99, no. B6, p. 12135–12141.
Merritts, D., and Vincent, K.R., 1989, Geomorphic response of coastal streams to low, intermediate, and high rates of uplift, Mendocino junction region, northern California: Geological Society of America Bulletin, v. 101, p. 1373–1388.
Moglen, G.E., and Bras, R.L., 1995, The importance of spatially heterogeneous erosivity and the cumulative area distribution within a basin evolution model: Geomorphology, v. 12, p. 173–185.
Molnar, P., and England, P., 1990, Late Cenozoic uplift of mountain ranges and global climate change: Chicken or egg?: Nature, v. 346, p. 29–34.
Montgomery, D.R., and Buffington, J.M., 1997, Channel-reach morphology in mountain drainage basins: Geological Society of America Bulletin, v. 109, p. 596–611.
Montgomery, D.R., and Foufoula-Georgiou, E., 1993, Channel network source representation using digital elevation models: Water Resources Research, v. 29, p. 1178–1191.
Pazzaglia, F.J., Gardner, T.W., and Merritts, D.J., 1998, Bedrock fluvial incision and longitudinal profile development over geologic time scales determined by fluvial terraces, *in* Tinkler, K.J., and Wohl, E.E., eds., Rivers over rock: Fluvial processes in bedrock channels: American Geophysical Union Geophysical Monograph 107, p. 207–236.
Prentice, C.S., Merritts, D.J., Beutner, E.C., Bodin, P., Schill, A., and Muller, J.R., 1999, Northern San Andreas fault near Shelter Cove, California: Geological Society of America Bulletin, v. 111, p. 512–523.
Rantz, S.E., 1968, Average annual precipitation and runoff in north coastal California: U.S. Geological Survey Hydrologic Investigations Atlas HA-298, scale 1:1 000 000, 1 sheet, 4 p.
Raymo, M.E., and Ruddiman, W.F., 1992, Tectonic forcing of late Cenozoic climate: Nature, v. 359, p. 117–122.
Rosenbloom, N.A., and Anderson, R.S., 1994, Evolution of the marine terraced landscape, Santa Cruz, California: Journal of Geophysical Research, v. 99, p. 14013–14030.
Seidl, M.A., and Dietrich, W.E., 1992, The problem of channel erosion into bedrock: Catena, supplement, v. 23, p. 101–124.
Sklar, L., and Dietrich, W.E., 1998, River longitudinal profiles and bedrock incision models: Stream power and the influence of sediment supply, *in* Tinkler, K.J., and Wohl, E.E., eds., Rivers over rock: Fluvial processes in bedrock channels: American Geophysical Union Geophysical Monograph 107, p. 237–260.
Slingerland, R., Willett, S.D., and Hovius, N., 1998, Slope-area scaling as a test of fluvial bedrock erosion laws [abs.]: Eos (Transactions, American Geophysical Union), v. 79, no. 45, p. F358.
Stock, J.D., and Dietrich, W.E., 1998, Channel incision by debris flows: A missing erosion law?: Eos (Transactions, American Geophysical Union), v. 79, no. 45, p. F366.
Stock, J.D., and Montgomery, D.R., 1999, Geologic constraints on bedrock river incision using the stream power law: Journal of Geophysical Research, v. 104, p. 4983–4993.
Talling, P.J., and Sowter, M.J., 1998, Erosion, deposition and basin-wide variations in stream power and bed shear stress: Basin Research, v. 10, p. 87–108.
Tarboton, D.G., Bras, R.L., and Rodriguez-Iturbe, I., 1991, On the extraction of channel networks from digital elevation data: Hydrological Processes, v. 5, p. 81–100.
Tucker, G.E., 1996, Modeling the regional-scale interaction of climate, tectonics and topography: Pennsylvania State University Earth System Science Center Technical Report 96-003, 267 p.
Tucker, G.E., and Bras, R.L., 1998, Hillslope processes, drainage density, and landscape morphology: Water Resources Research, v. 34, p. 2751–2764.
Tucker, G.E., and Slingerland, R.L., 1994, Erosional dynamics, flexural isostasy, and long-lived escarpments: A numerical modeling study: Journal of Geophysical Research, v. 99, p. 12229–12243.
Weissel, J.K., and Seidl, M.A., 1998, Inland propagation of erosional escarpments and river profile evolution across the southeast Australia passive continental margin, *in* Tinkler, K.J., and Wohl, E.E., eds., Rivers over rock: Fluvial processes in bedrock channels: American Geophysical Union Geophysical Monograph 107, p. 189–206.
Whipple, K.X., and Tucker, G.E., 1999, Dynamics of the stream-power river incision model: Implications for the height limits of mountain ranges, landscape response time scales, and research needs: Journal of Geophysical Research, v. 104, no. B8, p. 17661–17674.
Whipple, Kelin X., Hancock, Gregory S., and Anderson, Robert A., 2000, River incision into bedrock: Mechanics and relative efficacy of plucking, abrasion, and cavitation: Geological Society of America Bulletin, v. 112, p. 490–503.
Willgoose, G., 1994, A statistic for testing the elevation characteristics of landscape simulation models: Journal of Geophysical Research, v. 99, no. B7, p. 13987–13996.
Willgoose, G., Bras, R.L., and Rodriguez-Iturbe, I., 1990, A model of river basin evolution: Eos (Transactions, American Geophysical Union), v. 71, p. 1806–1807.
Wohl, E.E., 1998, Bedrock channel morphology in relation to erosional processes, *in* Tinkler, K.J., and Wohl, E.E., eds., Rivers over rock: Fluvial processes in bedrock channels: American Geophysical Union Geophysical Monograph 107, p. 133–151.
Wolman, M.G., and Miller, J.P., 1960, Magnitude and frequency of forces in geomorphic processes: Journal of Geology, v. 68, p. 54–74.

MANUSCRIPT RECEIVED BY THE SOCIETY MARCH 18, 1999
REVISED MANUSCRIPT RECEIVED SEPTEMBER 28, 1999
MANUSCRIPT ACCEPTED NOVEMBER 1, 1999

Printed in USA